Refining the anchor: optimizing the performance of cyclometallated ruthenium(II) dyes in p-type dye sensitized solar cells

Nathalie Marinakis, Cedric Wobill, Edwin C. Constable and Catherine E. Housecroft*

Department of Chemistry, University of Basel, BPR 1096, Mattenstrasse 24a, CH-4058 Basel, Switzerland

Email: catherine.housecroft@unibas.ch

Abstract

A comparison of the performances of p-type dye sensitized solar cells (DSCs) sensitized by three cyclometallated ruthenium(II) dyes differing in their anchoring domains is presented. The dyes are [Ru(bpy)$_2$(H**1**)] (H$_3$**1** = (4-(2-phenylpyridin-4-yl)phenyl)phosphonic acid) and the salts [^{n}Bu$_4$N][Ru(bpy)$_2$(**1**)] and [Ru(bpy)$_2$(H**2**)][PF$_6$] (H$_2$**2** = (4-(2-phenylpyridin-4-yl)phenyl)carboxylic acid). DSCs were fabricated with FTO/NiO working electrodes and either an I^-/I_3^-/MeCN or I^-/I_3^-/MeCN:EtCN (3:1 by volume) electrolyte. The results confirm the higher performance of dyes with a phosphonate versus carboxylic acid anchor, and reveal that [Ru(bpy)$_2$(H**1**)] (J_{SC} = 3.24 mA cm^{-2} and η = 0.116%) performs better than [Ru(bpy)$_2$(**1**)]$^-$. Electrochemical impedance spectroscopy (EIS) shows that a DSC with [Ru(bpy)$_2$(H**1**)] offers the lowest transport and recombination resistances and the shortest hole lifetime and diffusion length.

Keywords: p-type dye sensitized solar cell; ruthenium; cyclometallation; anchoring group

1. Introduction

There is significant interest in the use of cyclometallated ruthenium(II) complexes as sensitizers in dye-sensitized solar cells (DSCs) [1,2,3,4]. The special attraction of $[Ru(N^N)_2(C^N)]^+$ complexes (N^N = bidentate *N*,*N*′-ligand, C^N = cyclometallated *C*,*N*-ligand) as dyes originates in the orbital characteristics of the frontier molecular orbitals (HOMO and LUMO). The HOMO is localized on the Ru/C^N domain while the LUMO possesses N^N character [5] and therefore, the electronic properties of the complex can be modulated through functionalization of the C^N and C^N ligands. The discrete partitioning of N^N and $\{(C^N)_2Ir\}$ orbital character between the HOMO and LUMO in $[Ir(C^N)_2(N^N)]^+$ complexes has been exploited for the optimization of cyclometallated iridium(III) dyes in p-type DSCs [6]. Structurally, sensitizers for DSCs are characterized by the anchoring group (commonly a carboxylic or phosphonic acid) which binds the dye to the semiconductor surface [7] and ancillary groups which optimize electron transfer across the dye. Moving the anchor from the N^N to the C^N ligand in a $[Ru(N^N)_2(C^N)]^+$ cation converts the complex from being a sensitizer for an n-type to a p-type DSC [8–13]. A related p-type DSC sensitizer containing an $\{Ru^{II}(N^N^N)(C^N^N)\}$ core in which the cyclometallated ligand bears an anchoring carboxylic acid has also been reported [14].

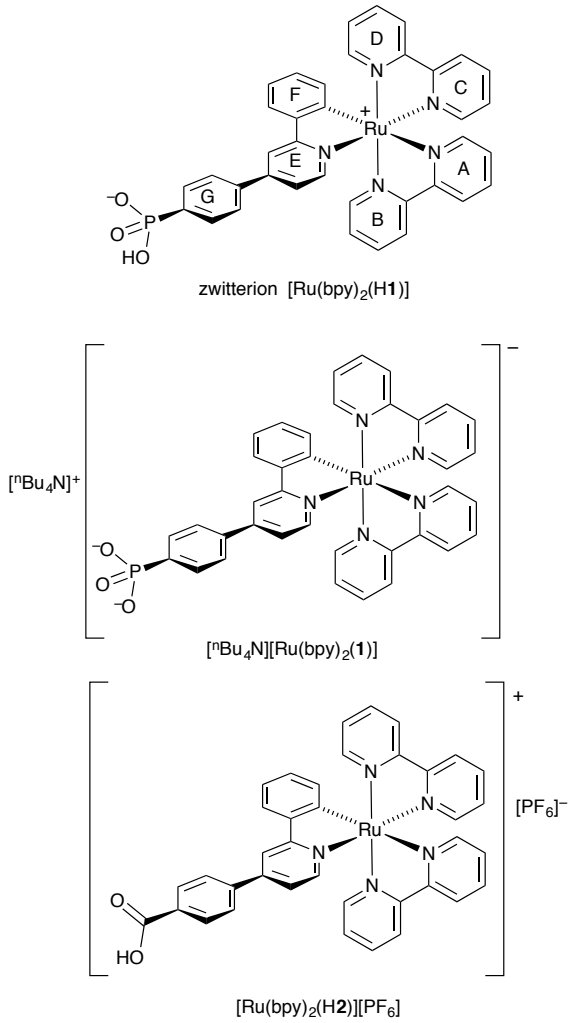

Scheme 1. Structures of the three dyes in this investigation.

Although cyclometallated ruthenium dyes (both for n-type and p-type DSCs) typically contain a carboxylic acid anchor [1,3,8–18] we have focused on the use of a phosphonic acids, based on the superior performance with respect to carboxylic acid anchors in n-type copper-sensitized DSCs [19]. Our initial investigations of p-type DSCs have used the zwitterionic dye [Ru(bpy)$_2$(H**1**)] (Scheme 1). Even though the structure of this dye has not been optimized, p-type DSCs containing FTO/NiO photocathodes sensitized with [Ru(bpy)$_2$(H**1**)] combined with an I^-/I_3^-/MeCN electrolyte show short-circuit current densities (J_{SC}) of between 3.38 and 4.13 mA cm^{-2} and photoconversion efficiencies (η) of

between 0.116 and 0.139% [12,20]. This sensitizer outperforms the reference dye P1 [12,21] (Scheme 2). The long-term stability of the DSC can be enhanced by changing the electrolyte solvent composition to a mixture of MeCN and EtCN (3 : 1 volume ratio), although at the expense of J_{SC} and η [20]. The performances of DSCs with [Ru(bpy)$_2$(H**1**)] are comparable to that of a DSC containing the more sophisticated dye shown in Scheme 3 (J_{SC} = 3.43 mA cm^{-2} and η = 0.104%) which is currently one of the best-performing cyclometallated ruthenium(II) dyes in p-type DSCs [8]. We now compare the performances of DSCs sensitized with [Ru(bpy)$_2$(H**1**)] with those containing the carboxylic acid anchored dye [Ru(bpy)$_2$(H**2**)][PF$_6$] (Scheme 1) and also investigate the effects of deprotonating [Ru(bpy)$_2$(H**1**)] and using [^{n}Bu$_4$N][Ru(bpy)$_2$(**1**)] (Scheme 1) as the dye.

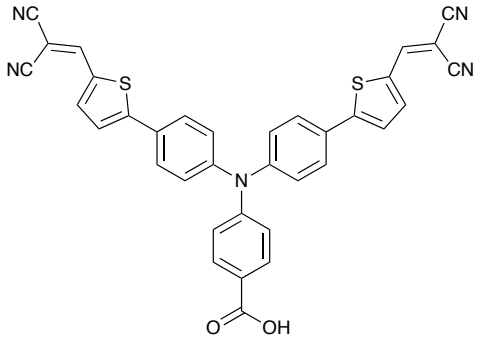

P1

Scheme 2. The structure of the reference p-type sensitizer P1.

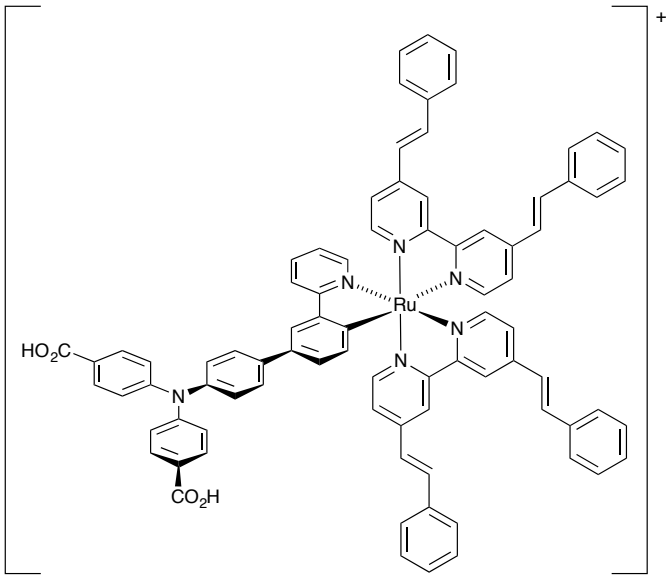

Scheme 3. A state-of-the-art p-type cyclometallated ruthenium(II) dye reported by Wu and coworkers [8].

2. Experimental

2.1 General

^{1}H and ^{31}P NMR spectra were recorded on a Bruker Avance III-500 spectrometer at 295 K. The ^{1}H chemical shifts were referenced with respect to residual solvent peaks (δTMS = 0), ^{11}B with respect to $BF_3{\cdot}Et_2O$, and ^{31}P with respect to 85% aqueous H_3PO_4. Mass spectra (LC-ESI-MS) were measured using a combination of Shimadzu (LC) and Bruker AmaZon X instruments.

[Ru(bpy)$_2$(H**1**)] and [Ru(bpy)$_2$(H**2**)][PF_6] were prepared as previously reported [12].

*2.1 [^{n}Bu$_4$N][Ru(bpy)$_2$(**1**)]*

[Ru(bpy)$_2$(H**1**)] (5.00 mg, 6.92 μmol, 1.0 eq.) was dissolved in MeOH (5.0 mL) and ^{n}Bu$_4$NOH (4.49 mg, 17.3 μmol, 2.5 eq.) was added as a 0.1 M solution in MeOH. The solution was stirred at room temperature for 2 h, after which the

solvent was removed under vacuum to leave [^{n}Bu$_4$N][Ru(bpy)$_2$(**1**)] with excess ^{n}Bu$_4$NOH. Attempts to remove the latter were unsuccessful (see text). ^{1}H NMR (500 MHz, CD$_3$OD) ^{1}H NMR (500 MHz, CD$_3$OD) δ / ppm 8.63 (dt, J = 8.3, 1.0 Hz, 1H, H^{A3}), 8.54 (m, 1H, H^{B3}), 8.47 (m, 1H, H^{C3}), 8.44 (m, 1H, H^{D3}), 8.31 (d, J = 2.0 Hz, 1H, H^{E3}), 8.17 (ddd, J = 5.7, 1.6, 0.7 Hz, 1H, H^{B6}), 8.07–7.97 (overlapping m, 4H, H$^{A4+F3+\text{ two of C4/B4/D4/C6}}$), 7.92 (overlapping m, 2H, H^{D6+A6}), 7.86 (m, 2H, H^{G2}), 7.79 (overlapping m, 2H, H$^{\text{two of C4/B4/D4/C6}}$), 7.71 (m, 2H, H^{G3}), 7.59 (dd, J = 6.0, 0.7 Hz, 1H, H^{E6}), 7.49 (ddd, J = 7.6, 5.4, 1.2 Hz, 1H, H^{A5}), 7.30–7.22 (overlapping m, 4H, H$^{B5+C5+D5+E5}$), 6.92 (ddd, J = 7.8, 7.2, 1.3 Hz, 1H, H^{F4}), 6.82 (td, J = 7.3, 1.3 Hz, 1H, H^{F5}), 6.45 (m, 2H, H^{F6}). ^{31}P{^{1}H} NMR (162 MHz, CD$_3$OD) δ / ppm +10.2. LC-ESI-MS *m/z*: 242.3 [^{n}Bu$_4$N]$^+$ (calc. 242.3), 724.2 [M + 2H]$^+$ (calc. 724.1). Satisfactory elemental analysis could not be obtained: see text.

2.2 *DSCs*

Working NiO electrodes were prepared in-house. An FTO glass plate (Solaronix TCO22-7, 2.2 mm thickness, sheet resistance =7 Ω square^{-1}) was cleaned by sonicating in surfactant (2% in milliQ water), and rinsed with milliQ water and EtOH. The surface was activated in a UV-O_3 system (Model 256-220, Jelight Company Inc) for 20 min. The plate was then dipped five times into a solution of [Ni(acac)$_2$] (ACROS) in MeCN (0.5 mM) and air dried after each dipping. A layer of NiO paste (Ni-Nanoxide N/SP, Solaronix) was screen-printed (90T, Serilith AG, Switzerland) onto the pretreated FTO plate, which was then placed in an EtOH chamber for 3 min to reduce surface irregularities and dried (125^{o}C heating plate, 6 min). In total, two cycles of screen printing were carried out and the resultant two-layer plate was sintered by gradually heating from room temperature to 350 °C over a period of 30 min, maintained at 350°C for 30 min,

then allowed to cool over 2 h to room temperature. The sintered FTO/NiO plates were then cut to form electrodes (1 cm × 2 cm). The thickness of the NiO layer (~1.0–2.5 μm) was confirmed using focused ion beam (FIB) scanning electron microscopy (REM-FEI Helios NanoLab 650).

DSCs were assembled as follows. The FTO/NiO electrodes were heated at 250°C (20 min), then cooled to 80°C before being immersed in an MeCN solution (0.3 mM) of P1 (Dyenamo AB) or EtOH solution (0.1 mM) of the selected ruthenium dye for 20 h. The electrodes were removed from the solutions, washed with EtOH, then dried in an N_2 stream. Commercial counter electrodes (Solaronix Test Cell Platinum Electrodes) were washed with EtOH and then heated at 450 °C (hot plate) for 30 min to remove volatile organic impurities. The DSCs were fabricated by combining working and counter electrodes using thermoplast hot-melt sealing foil (Solaronix, Meltonix 1170-25 Series, 60 μm thick) by heating while pressing them together. The electrolyte comprised I_2 (0.1 M), LiI (1 M) in MeCN or I_2 (0.1 M), LiI (1 M) in MeCN/propionitrile 3:1 and was added to the DSC by vacuum backfilling. The hole in the counter electrode was then closed using a hot-melt sealing foil and cover glass.

The solar cell measurements were made using duplicate unmasked cells with an active area of 0.237 cm^2. The DSCs were sun-soaked from the anode side for 20 min at 1 sun irradiation. The cell was then inverted and measured immediately with a LOT Quantum Design LS0811 instrument (100 mW cm^{-2} = 1 sun at AM1.5 and 23 °C) to obtain the current density–voltage (*J*–*V*) curves. The instrument software was set to a p-type measurement mode (inverted configuration), with a 360 ms settling time [12] and a voltage step of 5.3 mV. The voltage was scanned from negative to positive values.

2.3 Electrochemical impedance spectroscopy (EIS).

EIS measurements were carried out on a ModuLab® XM PhotoEchem photoelectrochemical measurement system from Solartron Analytical. The impedance was measured at the open-circuit voltage (V_{OC}) of the cell at different light intensities (590 nm) in the frequency range 0.05 Hz to 400 kHz using an amplitude of 10 mV. The impedance data were analysed using ZView® software from Scribner Associates Inc.

3 Results and discussion

*3.1 Synthesis and characterization of [$^{n}Bu_4N$][Ru(bpy)$_2$(**1**)]*

We have previously reported the synthesis and characterization of the zwitterion [Ru(bpy)$_2$(H**1**)] [12]. Treatment of a methanol solution of [Ru(bpy)$_2$(H**1**)] with an excess (2.5 equivalents) of $^{n}Bu_4NOH$ resulted in no visible change although the ^{1}H NMR spectrum of the ruthenium(II) complex revealed changes to the proton resonances assigned to the phenyl ring (ring G, Scheme 1) as shown in Fig. 1. A combination of COSY, HMQC, HMBC and NOESY methods were used to assign the signals in the spectrum of [Ru(bpy)$_2$(H**1**)] [12] and there are negligible changes to the signals arising from the A–F rings (Scheme 1) on adding base to a solution of [Ru(bpy)$_2$(H**1**)]. The shifts in the signals for protons H^{G2} and H^{G3} are consistent with deprotonation of the phosphonate group and the formation of [Ru(bpy)$_2$(**1**)]$^-$. In the ^{31}P NMR spectrum, a small shift to lower frequency (δ +10.8 to +10.2 ppm) is observed. The LC-ESI mass spectrum of the compound showed a peak at *m/z* 242.3 arising from the $[^{n}Bu_4N]^+$ and a peak envelope (dominated by the characteristic isotope pattern for ruthenium) at *m/z* 724.2, consistent with the $[M + 2H]^+$ ion. On their own, these data cannot be used to confirm the formation of the [Ru(bpy)$_2$(**1**)]$^-$

anion since both $[2H+Ru(bpy)_2(\mathbf{1})]^+$ and $[H+Ru(bpy)_2(H\mathbf{1})]^+$ would give the same ion in the mass spectrum. Evidence for the second proton loss from the phosphonate group and formation of $[^nBu_4N][Ru(bpy)_2(\mathbf{1})]$ relies upon the ^1H NMR spectroscopic data. When a CD_3OD solution of the compound was left to stand overnight, the ^1H NMR spectrum of the solution showed the spectroscopic signature of $[Ru(bpy)_2(H\mathbf{1})]$ (Fig. 1a). The protonation of $[Ru(bpy)_2(\mathbf{1})]^-$ to give $[Ru(bpy)_2(H\mathbf{1})]$, presumably by adventitious water in the solvent, is not unexpected based upon the values of $pK_a(1)$ and $pK_a(2)$ of 1.86 and 7.51, respectively, for phenylphosphonic acid [22]. We were unable to isolate pure solid $[^nBu_4N][Ru(bpy)_2(\mathbf{1})]$ for elemental analysis. Despite the problems associated with the isolation of $[^nBu_4N][Ru(bpy)_2(\mathbf{1})]$, we proceeded to use the compound (containing excess of $^nBu_4NOH$) as a dye. As discussed below, the reproducible performances for DSCs sensitized by $[^nBu_4N][Ru(bpy)_2(\mathbf{1})]$ differ significantly from those using the zwitterionic dye $[Ru(bpy)_2(H\mathbf{1})]$.

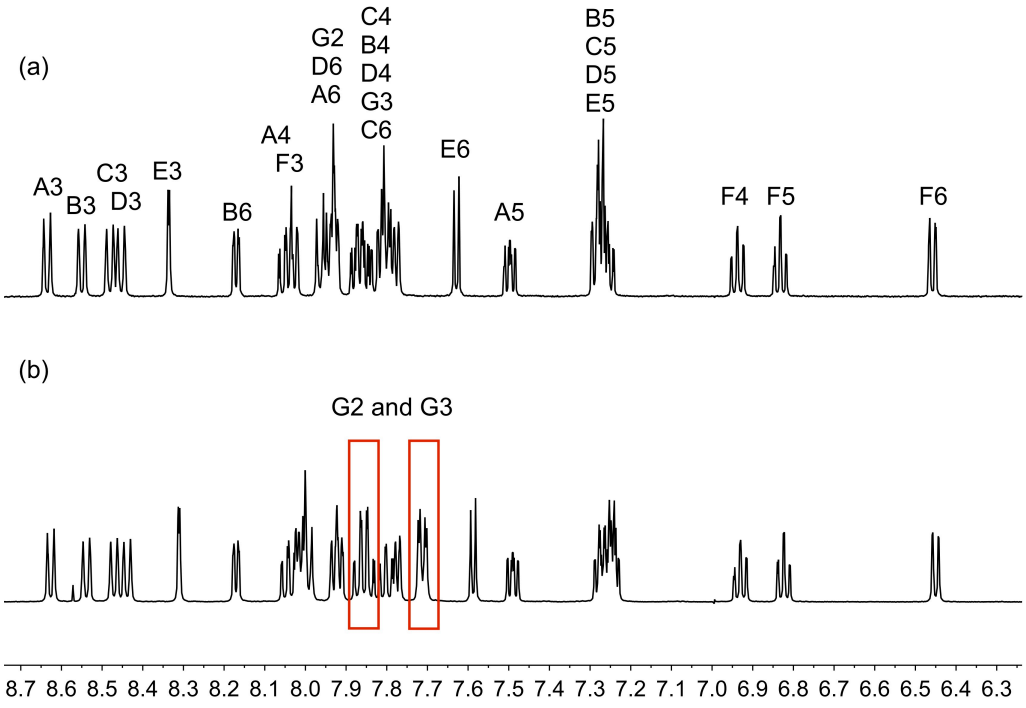

Fig. 1. 500 MHz ^{1}H NMR (CD_3OD) (a) [Ru(bpy)$_2$(H**1**)] and (b) [^{n}Bu$_4$N][Ru(bpy)$_2$(**1**)], emphasizing the changes in chemical shift of the signals for protons H^{G2} and H^{G3}.

3.2 DSC fabrication and performances

Photocathodes were prepared by screen-printing two layers of NiO paste onto FTO-coated glass pretreated with [Ni(acac)$_2$] [12]. After sintering (see Experimental section), the quality of the NiO surface was inspected using FIB measurements (Fig. 2). The thickness of the semiconductor layer (Fig. 2) was consistent with optimal photocathodes previously reported in p-type DSCs [21,23,24,25,26], and compatible with the limitations imposed by the diffusion length of a hole in the NiO [25].

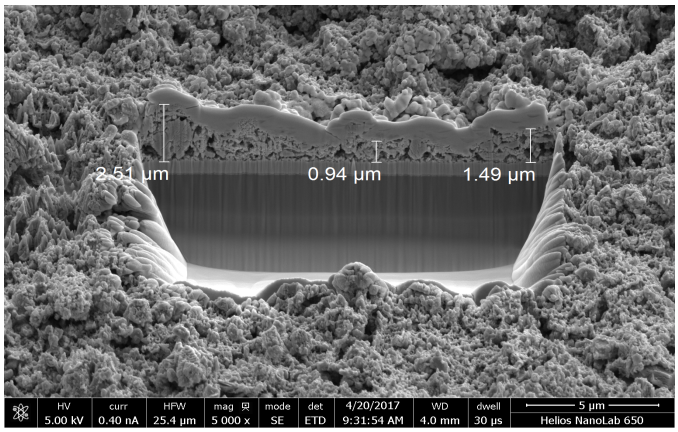

Fig. 2. FIB image of NiO electrode; a gallium beam (30 kV) cut into the NiO with a platinum layer is deposited on top of the NiO surface. The platinum layer was sputtered on the top surface as a protective layer against the ion beam.

Photocathodes were sensitized by immersion in ethanol solutions of [Ru(bpy)$_2$(H**1**)], freshly prepared [^{n}Bu$_4$N][Ru(bpy)$_2$(**1**)] or [Ru(bpy)$_2$(H**2**)][PF_6]. For reference, electrodes with absorbed dye P1 (Scheme 2) were also prepared. For each dye, duplicate DSCs were fabricated (see Experimental section). While

an electrolyte containing the I^-/I_3^- redox couple in MeCN is a common choice for p-type DSCs, we have demonstrated that use of a 3:1 MeCN:EtCN mixture yields improved long-term stability with respect to DSCs using only MeCN [20]. However, since this is only achieved with a small decrease in photoconversion efficiency (η), we decided to include DSCs with both solvent systems in the present investigation.

The performance parameters for the DSCs are given in Table 1 for MeCN and in Table 2 for the mixed solvent electrolyte, and *J*–*V* curves are shown in Figs. 3 and 4. The data for the DSCs with the reference dye P1 are similar to those we have previously reported [12,20] and, with an I^-/I_3^-/MeCN electrolyte, are consistent with data reported for P1 by Gibson and coworkers in their benchmarking investigation [21]. The reproducibility of cells sensitized by the zwitterion [Ru(bpy)$_2$(H**1**)] was confirmed, not only from the duplicate measurements in Tables 1 and 2, but also from a comparison of data in the present study with those in previous investigations [12,20]. With an I^-/I_3^-/MeCN electrolyte, the better performing cell exhibited values of J_{SC}, V_{OC} and η of 3.24 mA cm^{-2}, 102 mV and 0.116% (Table 1) compared to previously reported values of 3.38 mA cm^{-2}, 95 mV and 0.116% [12]. The change to the I^-/I_3^-/MeCN:EtCN electrolyte, resulted in values of J_{SC}, V_{OC} and η of 2.91 mA cm^{-2}, 99 mV and 0.099% for cell 2 (Table 2) compared to previously reported values of 2.86 mA cm^{-2}, 111 mV and 0.111% for in-house screen-printed electrodes [20]. Inspection of Figs. 3 and 4 and Tables 1 and 2 shows that, irrespective of the electrolyte solvent system, the trend in dye performances is the same: [Ru(bpy)$_2$(H**1**)] > [Ru(bpy)$_2$(**1**)]$^-$ ~ P1 > [Ru(bpy)$_2$(H**2**)]$^+$. Despite the problems in characterizing the bulk sample of [^{n}Bu$_4$N][Ru(bpy)$_2$(**1**)], it is clear that the

absorbed dye behaves differently from the neutral [Ru(bpy)$_2$(H**1**)]; this is supported by the EIS results discussed below. A second deprotonation of the phosphonate group in the cyclometallated ligand leads to a drop in J_{SC} with a consequent decrease in photoconversion efficiency. The data confirm that the phosphonate anchoring unit is superior to a carboxylic acid, with the best values of J_{SC} and V_{OC} being 1.38 mA cm^{-2} and 73 mV. Significantly, in an investigation of a series of sensitzers based on [Ru^{II}(bpy)$_3$] scaffolds on NiO p-type DSCs, Pellegrin *et al*. [27] demonstrated that dyes with phosphonic acid anchors performed better than those with carboxylic acid or catechol anchors. Our results are consistent with this trend. However, it is significant that the current densities achieved with the cyclometallated ruthenium sensitizers are higher than the values of J_{SC} reported for [Ru^{II}(bpy)$_3$] species (J_{SC} = 0.78 mA cm^{-2} for a phosphonic acid anchor, J_{SC} = 0.63 mA cm^{-2} for a carboxylic acid anchor) [27].

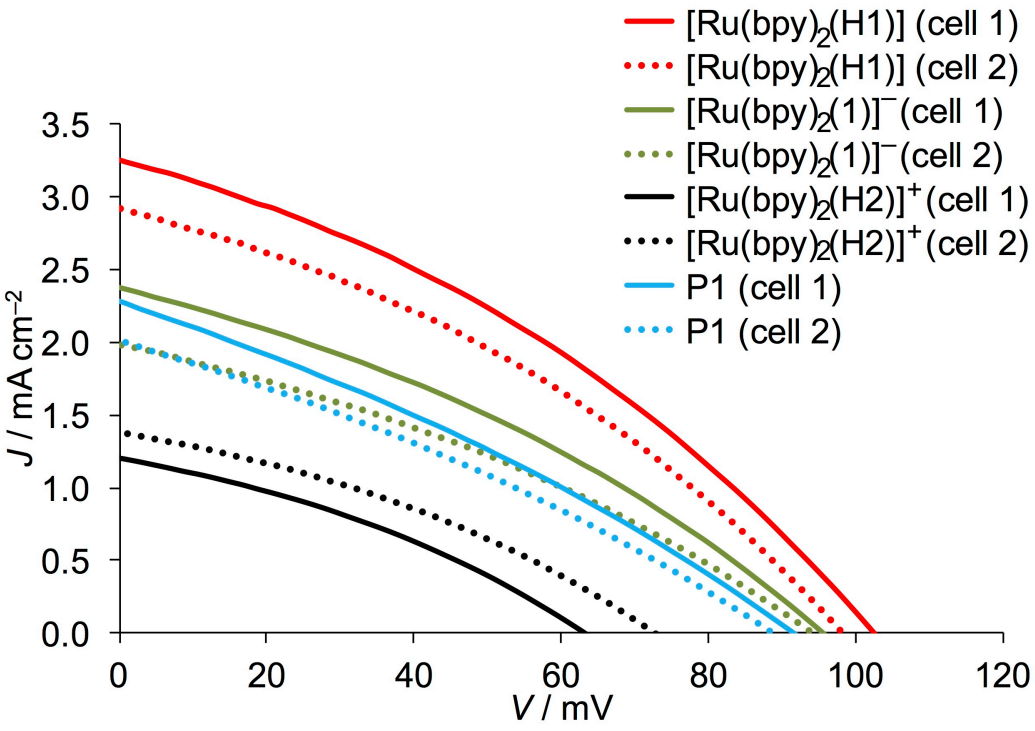

Fig. 3. *J*–*V* curves for duplicate p-type DSCs containing dyes [Ru(bpy)$_2$(H**1**)], [^{n}Bu$_4$N][Ru(bpy)$_2$(**1**)], [Ru(bpy)$_2$(H**2**)][PF$_6$] or P1 and an I$^-$/I$_3^-$/MeCN electrolyte. Measurements were made on the day the DSCs were assembled.

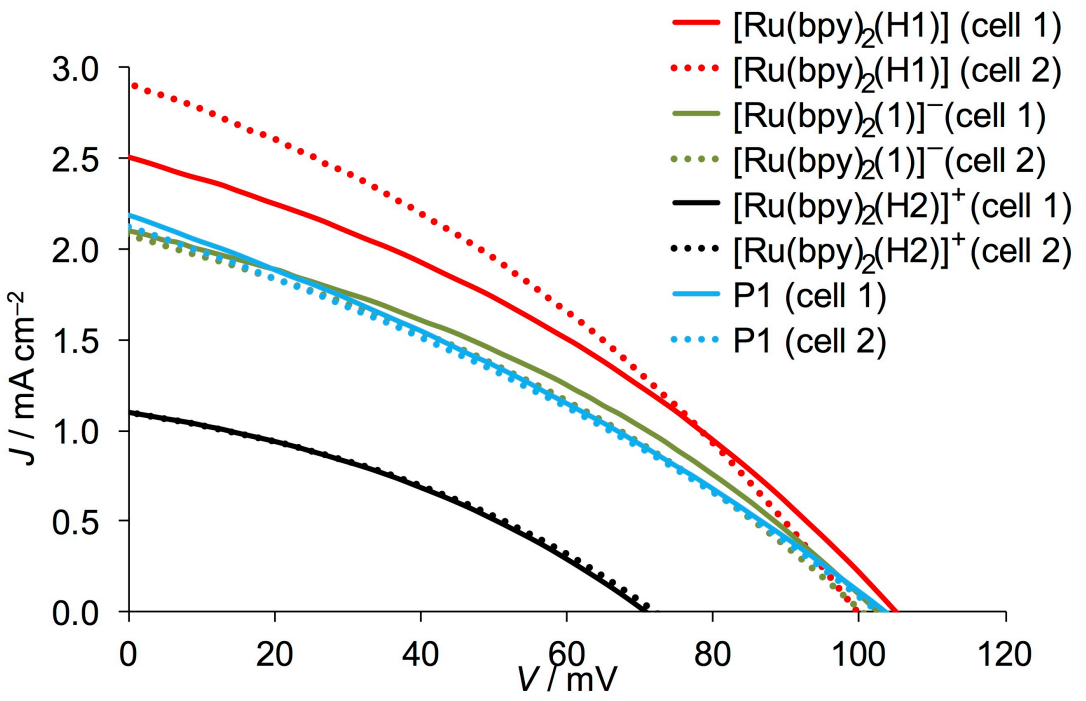

Fig. 4. *J*–*V* curves for duplicate p-type DSCs containing dyes [Ru(bpy)$_2$(H**1**)], [^{n}Bu$_4$N][Ru(bpy)$_2$(**1**)], [Ru(bpy)$_2$(H**2**)][PF$_6$] or P1 and an I^-/I_3^-/MeCN:EtCN (3:1) electrolyte. Measurements were made on the day the DSCs were assembled.

Table 1. Performance data on the day of sealing duplicate DSCs containing I^-/I_3^-/MeCN electrolyte (J_{SC} = short-circuit current density; V_{OC} = open-circuit voltage, *ff* = fill-factor, η = photoconversion efficiency).

Dye	DSC number	J_{SC} / mA cm^{-2}	V_{OC} / mV	*ff* / %	η / %
[Ru(bpy)$_2$(H**1**)]	cell 1	3.24	102	35	0.116
[Ru(bpy)$_2$(H**1**)]	cell 2	2.91	98	35	0.100
[Ru(bpy)$_2$(**1**)]$^-$	cell 1	2.37	95	34	0.076
[Ru(bpy)$_2$(**1**)]$^-$	cell 2	1.99	94	33	0.062
[Ru(bpy)$_2$(H**2**)]$^+$	cell 1	1.20	63	34	0.026
[Ru(bpy)$_2$(H**2**)]$^+$	cell 2	1.38	73	34	0.035
P1	cell 1	2.28	91	30	0.063

P1	cell 2	2.01	89	31	0.055

Table 2. Performance data on the day of sealing duplicate DSCs containing I^-/I_3^- /MeCN:EtCN (3:1) electrolyte.

Dye	DSC number	J_{SC} / mA cm^{-2}	V_{OC} / mV	*ff* / %	η / %
[Ru(bpy)$_2$(H**1**)]	cell 1	2.50	105	34	0.091
[Ru(bpy)$_2$(H**1**)]	cell 2	2.91	99	34	0.099
[Ru(bpy)$_2$(**1**)]$^-$	cell 1	2.10	102	35	0.075
[Ru(bpy)$_2$(**1**)]$^-$	cell 2	2.07	100	34	0.070
[Ru(bpy)$_2$(H**2**)]$^+$	cell 1	1.10	71	35	0.027
[Ru(bpy)$_2$(H**2**)]$^+$	cell 2	1.09	72	35	0.028
P1	cell 1	2.18	103	31	0.069
P1	cell 2	2.12	103	31	0.068

To assess the stability of the devices, their performances were remeasured 7 days after cell fabrication (Figs. S1 and S2 and Tables S1 and S2). The cells were stored in the dark under ambient conditions between measurements. For both electrolyte compositions, the DSCs sensitized with each cyclometallated ruthenium dye exhibited values of J_{SC}, V_{OC}, *ff* and η that changed little over time. In contrast, DSCs with P1 showed a loss in performance arising from decreases in J_{SC} from 2.28 to 1.60 mA cm^{-2} for cell 1 (MeCN) and from 2.18 to 1.54 mA cm^{-2} for cell 1 (MeCN/EtCN).

3.3 Electrochemical impedance spectroscopy

The internal processes and dynamics in a DSC can be thoroughly investigated by use of EIS [28,29,30]. The device is represented by a model based on an

equivalent electrical circuit composed of capacitances and resistances in accordance with the movement of the charge (holes) in the DSC. During the EIS measurement, AC voltages of different frequencies are applied to the DSC and the resulting current response is monitored with respect to both amplitude and phase shift. Results are typically expressed in Nyquist and Bode plots. We have previously described the features of the Nyquist plot [20] from which parameters including the recombination charge transfer resistance (R_{rec}), active layer surface chemical capacitance (C_{μ}), electron/hole transport resistance (R_t) and counter-electrode charge-transfer resistance (R_{Pt}) can be determined. Although, in principle, a Nyquist plot consists of three semi-circles, deconvolution to two semi-circles is more frequently observed for p-type DSCs as a result of the relative magnitudes of the recombination impedance and the ion diffusion impedance. The equivalent circuit used to fit the EIS data in the present investigation is shown in Fig. 5 [31]. In this study, a resistance-constant phase element (R-CPE) circuit was employed, with this choice of circuit being made because of the surface irregularities of the NiO electrode [32]. To account for this, the pre-factor term Q of the CPE was corrected using eq. (1), in which α is an empirical constant [33], to calculate the capacitance, C_{μ} [34].

$$C_{\mu} = \{(R_{rec})^{1-\alpha} Q\}^{1/\alpha} \qquad (1)$$

The equivalent electrical circuit used in this study is composed of a series resistance (R_s), the resistance (R_{FTO}) and capacitance (C_{FTO}) of the FTO/NiO interface, then an extended distributed element (DX-1) that consists of the sum of transport resistances (R_t), recombination resistance (R_{rec}) and capacitance (C_{μ}) of the NiO/electrolyte interface in series with a Warburg element (Z_d) and finally the resistance (R_{CE}) and capacitance (C_{CE}) of the counter electrode. The Nyquist plots for the DSCs with the three dyes are shown in Fig. 6; the expansion in Fig.

6(b) indicates that the model in Fig. 5 provides a good fit to the experimental data.

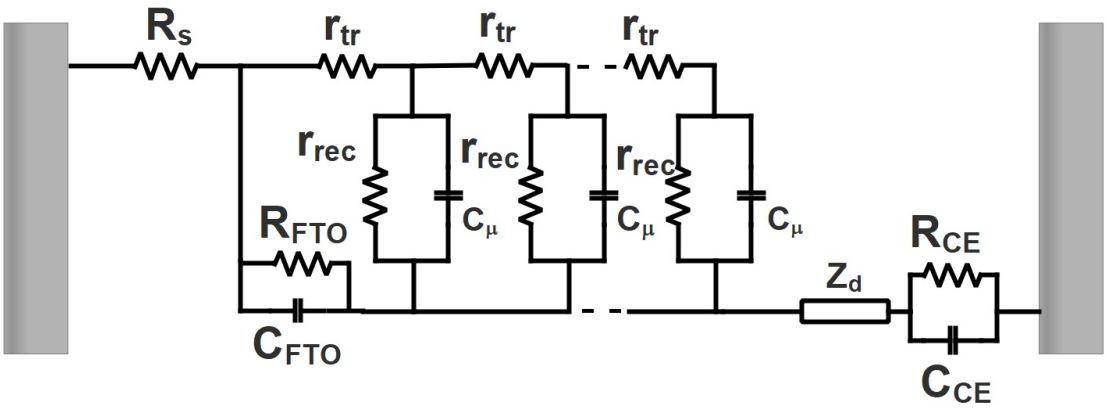

Fig. 5. Equivalent circuit used to fit the EIS data for NiO p-type DSCs in this study.

Table 3. EIS data obtained from measurements at a light intensity of 22 mW cm^{-2} of p-type DSCs containing FTO/NiO working electrodes, cyclometallated ruthenium(II) dyes, and I^-/I_3^- electrolyte in MeCN.

	R_s /Ω	R_{Pt} /Ω	C_{Pt} /μF	R_{rec} /Ω	R_t /Ω	C_μ / μF	τ_h /ms	τ_t /ms	L_d /μm	α[a]
[Ru(bpy)$_2$(H**1**)]	12.2	2.2	5.9	97.8	75.7	529.4	51.8	40.1	0.97	0.868
[Ru(bpy)$_2$(**1**)]$^-$	13.6	5.0	3.5	185.7	89.1	532.4	98.8	47.4	1.56	0.879
[Ru(bpy)$_2$(H**2**)]$^+$	15.1	1.5	4.1	632.6	83.2	850.8	538.2	70.8	5.70	0.847

[a]α is an empirical constant defined in eq. (1).

Using EIS, we have previously clarified the differences in behaviour between the sensitizers P1 and [Ru(bpy)$_2$(H**1**)] [20]. Here, we focus on the differences between the three cyclometallated dyes. EIS data for the better performing cell of each pair in Table 1 are summarized in Table 3 and Nyquist plots are presented in Fig. 6. From Table 1, we observe that values of V_{OC} for the DSCs sensitized with the [Ru(bpy)$_2$(H**1**)] (phosphonic acid anchor) are higher (102 mV) than those for [Ru(bpy)$_2$(**1**)]$^-$ (95mV) and [Ru(bpy)$_2$(H**2**)]$^+$ (73mV)

(carboxylic acid anchor). This is reflected in the EIS studies, where the value of R_t for the DSC with [Ru(bpy)$_2$(H**1**)] is lower than those for [Ru(bpy)$_2$(**1**)]$^-$ and [Ru(bpy)$_2$(H**2**)]$^+$. Values of R_{rec} in Table 3 follow the same trend as R_t, which is to be expected since the lower J_{SC} (Table 1) indicates fewer charge carriers being injected into the NiO, and therefore fewer holes are available for recombination, leading to a higher R_{rec}. The increase in capacitance, C_μ, from [Ru(bpy)$_2$(H**2**)]$^+$ to [Ru(bpy)$_2$(**1**)]$^-$ to [Ru(bpy)$_2$(H**1**)] is also consistent with [Ru(bpy)$_2$(H**1**)] being the best performing dye. As expected, the series resistance, R_s, is constant (Table 3).

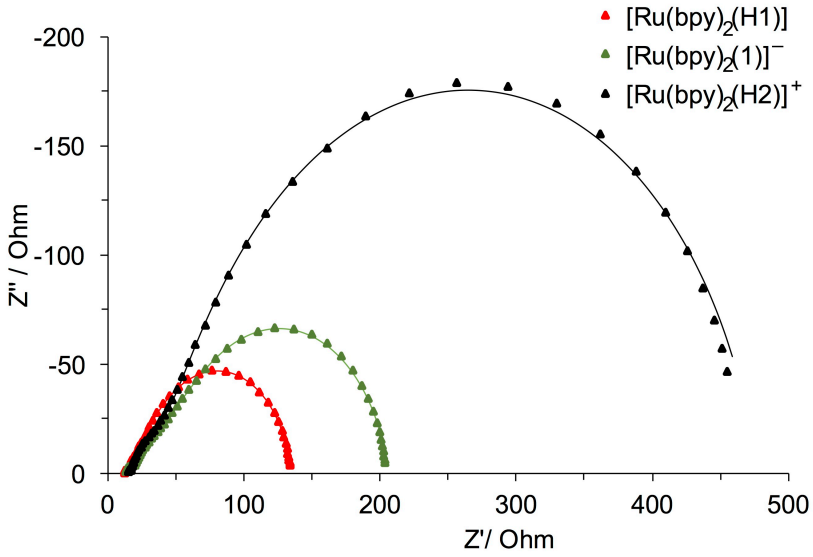

(a)

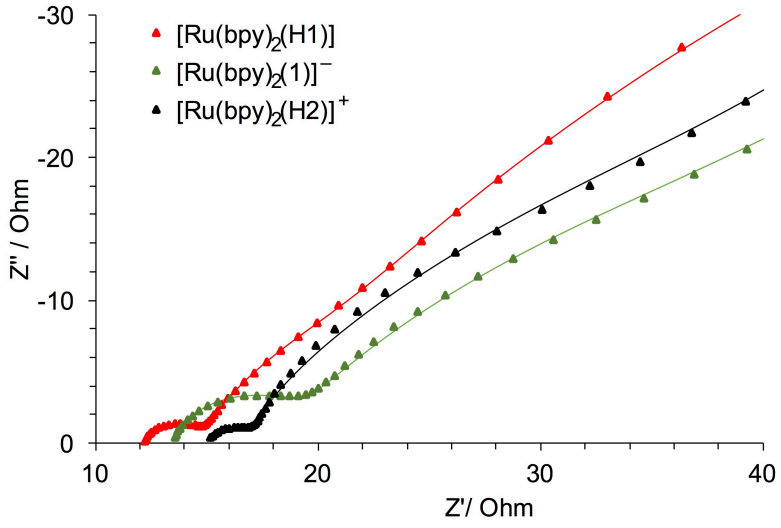

(b)

Fig. 6. (a) Nyquist plots of p-type DSCs sensitized with [Ru(bpy)$_2$(H**1**)], [^{n}Bu$_4$N][Ru(bpy)$_2$(**1**)] and [Ru(bpy)$_2$(H**2**)][PF$_6$]; the electrolyte is I^-/I_3^-/MeCN. Fitted curves are shown as solid lines. (b) Expansion of the high frequency region.

The EIS parameters were calculated using eq. 2–4 [35,36,37].

$$\tau_h = R_{rec}C_\mu \qquad (2)$$

$$L_d = d(R_{rec}/R_t)^{1/2} \qquad (3)$$

$$\tau_t = R_tC_\mu \qquad (4)$$

where d is the thickness of the semiconductor in μm. The hole lifetime, τ_h, can be calculated using eq. (2). Table 3 shows that the best performing dye [Ru(bpy)$_2$(H**1**)] has the shortest hole lifetime and the shortest hole diffusion length, L_d. Together these parameters contribute to a good performing DSC. Since the hole lifetime is inversely related to the value of the maximum frequency f_{max} [38], it follows that the trend in values of τ_h can also be seen in the Bode plot (Fig. 7). The cell sensitized with [Ru(bpy)$_2$(H**2**)]$^+$ has the lowest frequency peak position (f_{max} = 1.99 Hz) compared to the cells sensitized with [Ru(bpy)$_2$(**1**)]$^-$ and [Ru(bpy)$_2$(H**1**)] (f_{max} = 5.0 and 6.3 Hz, respectively).

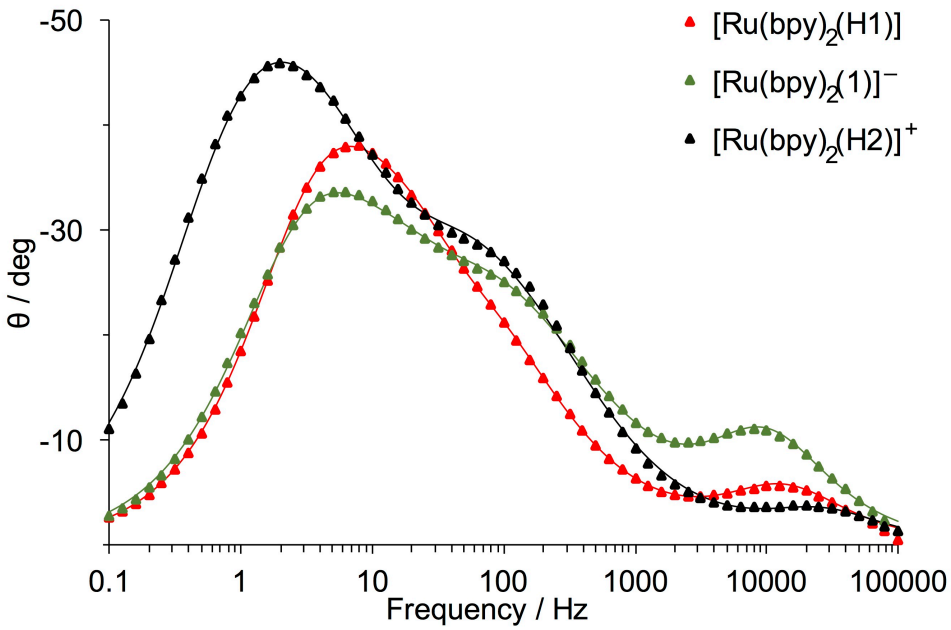

Fig. 7. Bode plots of p-type DSCs sensitized with [Ru(bpy)$_2$(H**1**)], [^{n}Bu$_4$N][Ru(bpy)$_2$(**1**)] and [Ru(bpy)$_2$(H**2**)][PF$_6$]; the electrolyte is I^-/I_3^-/MeCN. Fitted curves are shown as solid lines.

The diffusion length is calculated using eq. (3). For the DSC sensitized with [Ru(bpy)$_2$(H**2**)]$^-$, the high R_{rec} leads to a high L_d which is consistent with the low J_{SC} of the DSC (Table 1). The transport time is calculated from eq. (4) and the trends τ_t in Table 3 are consistent with the performances of the dyes (Table 1).

4. Conclusions

A comparison of the performances of three cyclometallated ruthenium(II) sensitizers in p-type DSCs has revealed that binding the dye to a NiO working electrode through a phosphonic acid anchoring domain leads to enhanced values of J_{SC} and photoconversion efficiencies (3.24 mA cm^{-2} and η = 0.116% for the best performing DSC) with respect to a comparable dye bearing a carboxylic acid anchor (J_{SC} = 1.38 mA cm^{-2}, η = 0.035%). In the zwitterionic dye [Ru(bpy)$_2$(H**1**)], the phosphonic acid anchoring group is in a monodeprotonated state. Removal of the second proton to give [Ru(bpy)$_2$(**1**)]$^-$ results in a dye with a lower J_{SC} and overall photoconversion efficiency than [Ru(bpy)$_2$(H**1**)]. A change from an I^-/I_3^-/MeCN to I^-/I_3^-/MeCN:EtCN (3:1 by volume) electrolyte has only a small influence on device performance, and all DSCs exhibit good stability over a period of 7 days. EIS studies have shown that of the three ruthenium sensitizers studied, dyes with phosphonic acid anchors are superior to that bearing a carboxylic acid anchor. The DSC containing [Ru(bpy)$_2$(H**1**)] combined with an I^-/I_3^-/MeCN electrolyte exhibits the lowest transport and recombination resistances, the shortest hole lifetime and the shortest hole diffusion length.

Acknowledgements

We thank the Swiss National Science Foundation (Grant number 200020_144500) and the University of Basel for financial support. Frederik J. Malzner (Department of Chemistry, University of Basel) and Dr Thilo Glatzel (Department of Physics, University of Basel) are gratefully acknowledged for thought-provoking discussions. FIB images were recorded at the Nano Imaging Lab (Swiss Nanoscience Institute, University of Basel).

Supporting information

Tables S1 and S2 give performance data and Figs. S1 and S2 show *J*–*V* curves for DSCs 7 days after sealing duplicate DSCs containing I^-/I_3^-/MeCN and I^-/I_3^-/MeCN:propionitrile (3:1) electrolytes, respectively.

References

1 K.C.D. Robson, P.G. Bomben and C.P. Berlinguette, Dalton Trans. 41 (2012) 7814.

2 P.G. Bomben, K.C.D. Robson, B.D. Koivisto and C.P. Berlinguette, *Coord.* Chem. Rev. 256 (2012) 1438.

3 A. Colombo, C. Dragonetti, A. Valore, C. Coluccini, N. Manfredi and A. Abbotto, Polyhedron 82 (2014) 50.

4 S. Soman, Y Xie, T.W. Hamann, Polyhedron 82 (2014) 139.

5 P.G. Bomben, K.C.D. Robson, P. A. Sedach, C.P. Berlinguette, Inorg. Chem. 48 (2009) 9631.

6 A. Sinopoli, C.J. Wood, E.A. Gibson, P.I.P. Elliott, Dyes and Pigments 140 (2017) 269.

7 L. Zhang, J.M. Cole, ACS Appl. Mater. Interfaces 7 (2015) 3427.

8 M. He, Z. Ji, Z. Huang, Y. Wu, J. Phys. Chem. C 118 (2014) 16518.

9 Z. Ji, G. Natu, Y. Wu, ACS Appl. Mater. Interfaces 5 (2013) 8641.

10 Z. Ji, G. Natu, Z. Huang, O. Kokhan, X. Zhang, Y. Wu, J. Phys. Chem. C 116 (2012) 16854.

11 Z. Ji, Y. Wu, J. Phys. Chem. C 117 (2013) 18315.

12 F. Brunner, N. Marinakis, C. Wobill, M. Willgert, C.D. Ertl, T. Kosmalski, M. Neuburger, B. Bozic-Weber, T. Glatzel, E.C. Constable, C.E. Housecroft, J. Mater. Chem. C 4 (2016) 9823.

13 Z. Ji, M. He, Z. Huang, U. Ozkan, Y. Wu J. Am. Chem. Soc. 135 (2013) 11696.

14 C.J. Wood, K.C.D. Robson, P.I.P. Elliott, C. P. Berlinguette, E.A. Gibson, RSC Adv. 4 (2014) 5782.

15 J.-F. Huang, J.-M. Liu, P.-Y. Su, Y.-F. Chen, Y. Shen, L.-M. Xiao, D.-B. Kuang, C.-Y. Su, Electrochim. Acta 174 (2015) 494.

16 T. Bessho, E. Yoneda, J.-H. Yum, M. Guglielmi, I. Tavernelli, H. Imai, U. Rothlisberger, M.K. Nazeeruddin, M. Grätzel, J. Am. Chem. Soc. 131 (2009) 5930.

17 C.-H. Siu, C.-L. Ho, J. He, T. Chen, P. Majumda, J. Zhao, H. Li, W.-Y. Wong, Polyhedron 82 (2014) 71.

18 T. Funaki, N. Onozawa-Komatsuzaki, K. Kasuga, K. Sayama, H. Sugihara, Inorg. Chem. Comm. 35 (2013) 281.

19 C. E. Housecroft, E. C. Constable, Chem. Soc. Rev. 44 (2015) 8386.

20 N. Marinakis, M. Willgert, E.C. Constable, C.E. Housecroft, Sustain. Ener. Fuels 1 (2017) 626.

21 C.J. Wood, G.H. Summers, C.A. Clark, N. Kaeffer, M. Braeutigam, L.R. Carbone, L. D'Amario, K. Fan, Y. Farré, S. Narbey, F. Oswald, L.A. Stevens, C.D.J. Parmenter, M.W. Fay, A. La Torre, C.E. Snape, B. Dietzek, D. Dini, L. Hammarström, Y. Pellegrin, F. Odobel, L. Sun, V. Artero, E.A. Gibson, Phys. Chem. Chem. Phys. 118 (2016) 10727.

22 Metal Phosphonate Chemistry: From Synthesis to Applications, eds. A. Clearfield and K. Demadis, RSC Publishing, Ch. 5, p. 166

23 S. Powar, T. Daeneke, M. T. Ma, D. Fu, N. W. Duffy, G. Götz, M. Weidelener, A. Mishra, P. Bäuerle, L. Spiccia, U. Bach, Angew. Chem. Int. Ed. 52 (2013) 602.

24 S. Sheehan, G. Naponiello, F. Odobel, D. P. Dowling, A. Di Carlo, D. Dini, J. Solid State Electrochem. 19 (2015) 975.

25 F. Odobel, Y. Pellegrin, J. Phys. Chem. Lett. 4 (2013) 2551.

26 V. Novelli, M. Awais, D. P. Dowling, D. Dini, J. Anal. Chem. 6 (2015) 176.

27 Y. Pellegrin, L. Le Pleux, E. Blart, A. Renaud, B. Chavillon, N. Szuwarski, M. Boujtita, L. Cario, S. Jobic, D. Jecquemin, F. Odobel, J. Photochem.and Photobiol. A 219 (2011) 235.

28 F. Fabregat-Santiago, G. Garcia-Belmonte, I. Mora-Seró, J. Bisquert, Phys. Chem. Chem. Phys. 13 (2011) 9083.

29 J. Bisquert, J. Electroanal. Chem. 646 (2010) 43.

30 F. Fabregat-Santiago, J. Bisquert, E. Palomares, L. Otero, D. Kuang, S. M. Zakeeruddin, M. Grätzel, J. Phys. Chem. C 111 (2007) 6550.

31 H. Liu, W. Xiang, H. Tao, J. Photochem. Photobiol. A 344 (2017) 199.

32 P. Córdoba-Torres, Electrochim. Acta 225 (2017) 592.

33 C. Cramer, S. Brunklaus, Y. Gao, K. Funke, J. Phys. Condens. Matter, 15, 2003, S2309.

34 M.R. Shoar Abouzari, F. Berkemeier, G. Schmitz, D. Wilmer, Solid State Ionics 180 (2009) 922.

35 F. Fabregat-Santiago, J. Bisquert, G. Garcia-Belmonte, G. Boschloo, A. Hagfeldt, Solar Energy Mater. Solar Cells 87 (2005) 117.

36 J. Halme, P. Vahermaa, K. Miettunen, P. Lund, Adv. Mater. 22 (2010) E210.

37 Z. Huang, G. Natu, Z. Ji, M. He, M. Yu, Y. Wu, J. Phys. Chem. C 116 (2012) 26239.

38 P. Ho, L. Q. Bao, K. S. Ahn, R. Cheruku, J. H. Kim, Synthetic Metals 217 (2016) 314.